Supporting Information

Disruption of electrospinning due to water condensation into the Taylor cone

*Catherine G. Reyes and Jan P. F. Lagerwall**

Department of Physics and Materials Science, University of Luxembourg,
162A, avenue de la Faiencerie L-1511 Luxembourg, Luxembourg

*Email: jan.lagerwall@lcsoftmatter.com
Phone: (+352) 46 66 44 6219
Fax: (+352) 46 66 44 36219

1 Movies

Movies S1, S2 and S3 show the evolution of non-coaxial Taylor cones from the solution containing only PVP and anhydrous ethanol spun at 55% RH, 65% RH and at 72% RH respectively, at $\sim$ 23 °C.
Movie S4 shows the corresponding stable 5CB–PVP Taylor cone from where the screenshot in Figure 2(a) (found in the main text) was taken.
Movie S5 shows the corresponding unstable and distorted 5CB–PVP Taylor cone from where the screenshot in Figure 2(b) (found in the main text) was taken.
Movies S6 and S7 show the evolution of coaxial Taylor cones formed from co-flowing three nematic LCs (S6: 5CB; S7:E7 and ROTN-403) into the PVP-in-anhydrous-ethanol solution (spun on its own in Movies S1-S3) to form fibers with polymer-sheath–LC-core geometry in 64% RH.
Movies S8, S9, and S10 show the differences in how each LC–PVP–ethanol droplet wet the orifice of the metal capillary before dripping (S9: 5CB; S10: E7; S11: ROTN-403).
Movie S11 shows how a hanging 5CB–PVP–ethanol droplet from a glass capillary quickly gels, becoming sticky and elastic, when exposed to 63% RH. The gelled drop is briefly poked by a needle and rebounds.

2 Liquid crystal miscibility with different solvents

Figure S1 qualitatively compares the solubility of the three liquid crystals (LCs) considered in our study (5CB, E7, and ROTN-403) in six common laboratory solvents. The solvent to LC ratio is 5:1 for each bottle shown in (a) and (c). If the LC is completely soluble in the solvent it appears as a single, isotropically clear, phase. Apart from all LCs being insoluble in water and ethylene glycol, we see that 5CB (molecular structure in Figure S2), with the lowest clearing temperature, dissolves in the third most polar solvent according to the chart in (b), then E7 partially dissolves in the fourth, and ROTN-403 in the fifth.

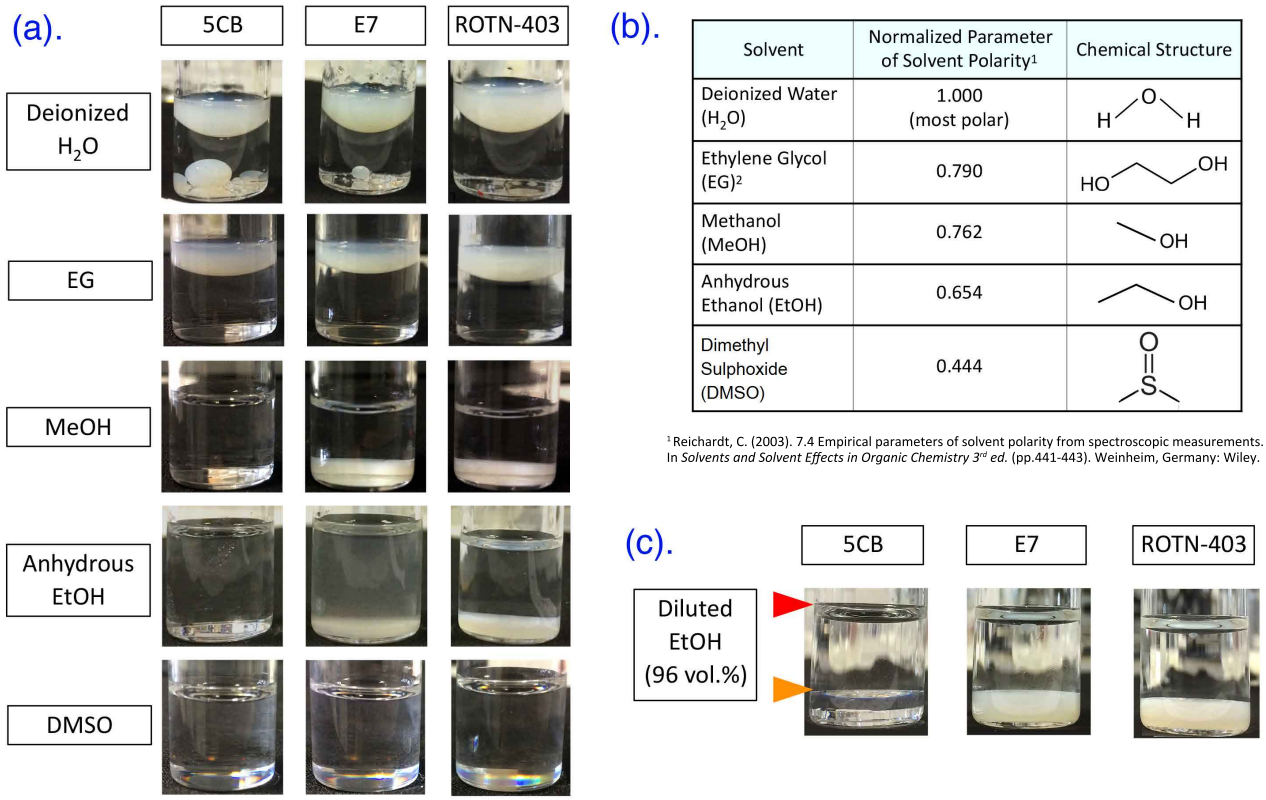

(b).

Solvent	Normalized Parameter of Solvent Polarity[1]	Chemical Structure
Deionized Water (H_2O)	1.000 (most polar)	
Ethylene Glycol (EG)[2]	0.790	
Methanol (MeOH)	0.762	
Anhydrous Ethanol (EtOH)	0.654	
Dimethyl Sulphoxide (DMSO)	0.444	

[1] Reichardt, C. (2003). 7.4 Empirical parameters of solvent polarity from spectroscopic measurements. In *Solvents and Solvent Effects in Organic Chemistry 3rd ed.* (pp.441-443). Weinheim, Germany: Wiley.

Figure S1: The LCs 5CB, E7 and ROTN-403 in deionized water (H_2O), ethylene glycol (EG), anhydrous methanol (MeOH), anhydrous ethanol (EtOH), and dimethyl sulfoxide (DMSO) are shown ($\sim$ 23 °C, $\sim$25% RH) in (a). The chemical structures and normalized parameters of solvent polarity (according to Reichardt [1,2]) for each of the non-diluted solvents in (a) are shown in (b). Image (c) shows that 5CB, unlike E7 and ROTN-403, forms two immiscible and coexisting isotropic phases at room temperature in diluted ethanol (96 vol.% EtOH), indicated by the red and orange triangles pointing to their respective interfaces.

An exceptional behavior is seen in (c), with 5CB in diluted ethanol which has $\sim$4% water: while the 5CB is completely dissolved and the nematic phase disappears, the result is two coexisting isotropic phases with different compositions (the meniscus of each phase is indicated by the red and orange arrows, respectively). In (c) the E7 LC phase appears slightly cloudy, indicating partial miscibility, but the ROTN-403 phase is still intact, and strongly scatters without having a diffuse interface in the solvent.

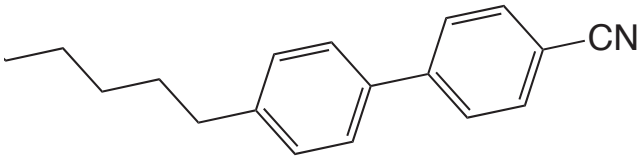

Figure S2: The molecular structure of 5CB.

3 Polarizing microscopy investigations of the core–sheath interface

To gain a better understanding of the phase separation taking place at the mixing front where the pure 5CB comes into contact with the ethanolic PVP solution during electrospinning in humid air, we recreate this situation under controlled conditions in a flat capillary for study

in the polarizing microscope (POM), see Figure S3. The capillary is first half-filled with pure 5CB by capillary suction, and then the 5CB end is dipped into a 12.5 mass-% PVP solution in aqueous ethanol, originally prepared with 3 vol.% water in anhydrous ethanol to emulate the conditions of electrospinning with water condensation from the air. Capillary suction then fills the rest of the capillary with the PVP solution. The capillary is immediately sealed and transferred to the POM, where we study the interface where 5CB meets the aqueous-ethanolic PVP solution.

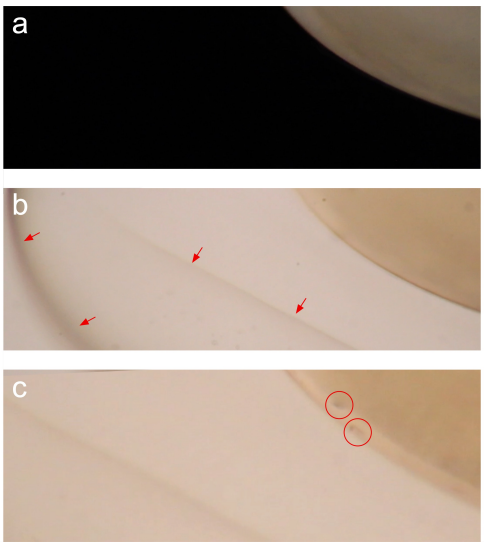

Figure S3: Polarizing optical microscopy (POM) investigation of the mixing front between pure 5CB (from the right) and a 12.5% (by mass) PVP solution (from the left) in aqueous ethanol (3 vol.% water in anhydrous ethanol). Panel (a) is taken between crossed polarizers, showing that only the top right-hand corner is nematic. Panel (b) shows the same scene, with the same focus, without analyzer, revealing through boundary lines (highlighted with arrows)
that there are multiple phases in the isotropic regime. Panel (c) is similar to (b) but with slightly different focus, revealing a heterogeneous character with dark aggregates (highlighted with red circles) in the nematic region, possibly due to PVP precipitating in these areas. Scale bar: 200 μm.

In Figure S3 we easily distinguish the nematic region from the isotropic, as the former is bright between crossed polarizers whereas the latter is black. By removing the analyzer (panel b), we find that there are at least two large phase boundaries (highlighted by red arrows) also within the isotropic region, as well as multiple faint boundaries of small nucleating phases in one of the main isotropic phases. As discussed in our study focusing specifically on this phase separation phenomenon,[3] strong flows occur at each such phase boundary since the two adjacent phases have very different compositions but develop from a single liquid phase. The interface is thus very dynamic, with multiple phase separation events taking place as a result of the concentration gradient. Moreover, by slightly changing the focus (Figure S3c) we see some diffuse aggregates (highlighted with red circles) in the nematic regime, possibly indicating PVP precipitating from solution in this regime dominated by 5CB, which is a non-solvent for the polymer.

4 Long-term study of phase separation in controlled 5CB-ethanol-PVP-water mixtures

The miscibility gap in the ternary phase diagram between 5CB, ethanol and water (see Figure 6 in the main text) causes the phase separation between two isotropic liquid phases of different composition between the three components, explaining the observations in Figure S3. One phase is ethanol-rich and 5CB-poor, the other has the inverse relationship, although ethanol-'poor' here still means on the order of 50 mol-% ethanol, (Figure 6 in the main text). The miscibility gap and consequent phase separation exists also in the pure ethanol–5CB phase diagram, but there it occurs only at very low temperatures. Adding just a small amount of water has the drastic consequence of raising the miscibility gap to room temperature and beyond, thereby significantly impacting the behavior of this LC-polymer-solvent mixture during electrospinning.

A question of relevance is if the PVP has a preference for either of the two isotropic phases that form during the phase separation. We would expect it to primarily reside in the ethanol-rich component, as 5CB is not a solvent for PVP. To test for this, we prepare a controlled mixture, consisting of a 12.5 mass-% solution of PVP in slightly aqueous ethanol solution (3 vol.% water and 97 vol.% anhydrous ethanol) to which we add 5CB at a mole fraction of 20%. This is based on the corresponding phase diagram established in reference,[3] reproduced for convenience in Figure 6 in the main text, where we target the middle of the miscibility gap to achieve roughly equal volumes of each isotropic phase. The mass fraction of PVP added is based on the typical mixture compositions of ethanol and PVP used during electrospinning experiments.

The mixture containing the four components (PVP, 5CB, ethanol and water) is stirred vigorously and then filled into a 50 mL separatory funnel, within which a macroscopic separation into two volumes immediately occurs, see Figure S4a. However, the top phase shows significant scattering, suggesting strong heterogeneity within. Interestingly, over a course of a day, the scattering moves to the bottom phase (Figure S4b) and two days later both the top and the bottom phases scatter strongly. These radical changes at the beginning of the process show that the system is very far from equilibrium and it takes time to reach an equilibrium state. In our earlier study, without the PVP, the phase separation into two clear isotropic phases occurred rapidly, in less than half an hour, at these conditions.[3] It thus seems that the presence of PVP, which has a high molar mass and an affinity for both ethanol and water molecules, significantly slows down the trajectory towards the final macroscopic phase separation, creating a very large number of internal boundaries within each phase. Thus, complete separation such that two clear and homogeneously isotropic phases form takes many days to stabilize.

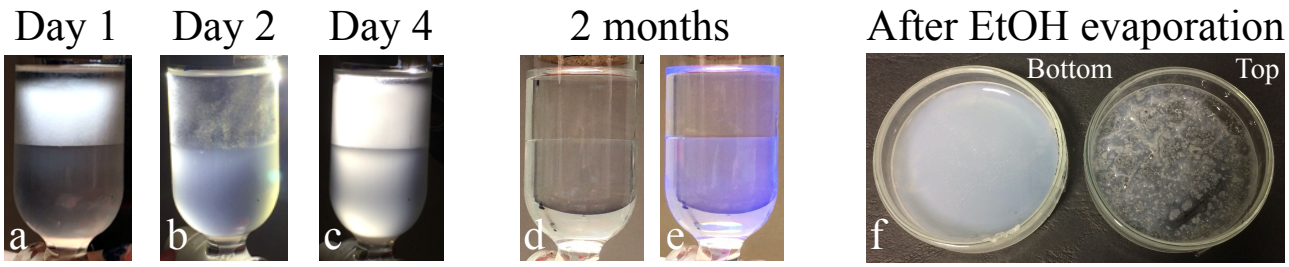

Figure S4: Phase separation of a controlled mixture containing 20 mol% 5CB in aqueous ethanol (3 vol.% water and 97 vol% anhydrous ethanol), the latter containing 12.5 mass-% PVP prior to the 5CB addition, as seen over time in a separatory funnel. A macroscopic separation into two main volumes is immediately seen, but strong scattering in either or both phases occurs during the first days (a–c; white light from behind), indicating significant heterogeneity. After 2 months of settling, two clear isotropic phases have formed (d). By illuminating with 366 nm UV light (e), we can see that most of the 5CB resides in the lower phase, as 5CB fluoresces under these illumination conditions. This is further confirmed once both clear phases are extracted into separate Petri dishes, and the excess ethanol is evaporated (f); the bottom phase remains largely nematic, suggesting a significant quantity of 5CB present, while the top phase contains primarily dried PVP polymer.

We leave the sample standing for two months, allowing the system to reach equilibrium, with two clear isotropic phases residing on top of each other at the end, see Figure S4d. By illuminating the sample with 366 nm UV light we confirm that the 5CB, which shows fluorescence at this irradiation wavelength, resides primarily in the lower phase, see Figure S4e. Note that this is the 5CB-*rich* phase, containing about 45 mol% 5CB according to the phase diagram in Figure 6 in the main text (the composition is found at the crossing of the right binodal, connecting points (1) and (2), with room temperature, about 20°C), it is not pure 5CB. The lower phase still contains a significant fraction of ethanol, explaining why it is isotropic and not nematic at room temperature. Likewise, the upper phase contains 5CB, albeit less than the lower phase.

We separate the phases into two individual vials, leaving a fraction of each in open Petri dishes in the fumehood, and the excess ethanol is allowed to evaporate, the result shown in Figure S4f. The dish containing the lower phase is now nematic, as the non-volatile 5CB remains after the ethanol has been evaporated. The dish containing the top phase shows a gel-like residue of PVP interspersed with a small fraction of 5CB that resided in this phase. It appears that once equilibrium is established, over a time scale of weeks to months, the majority of the PVP ends up in the ethanol-rich phase, as might be expected, but there is probably also some PVP in the 5CB-rich phase, as also this contains ethanol. The experiment in Figure S4 shows that, even if an equilibrium situation with two well-defined phases exists, it takes weeks to reach a state where the two phases are macroscopically separated. Considering the time scale that liquid resides in the Taylor cone during electrospinning, before reaching the jet, the mixing components remain far from equilibrium, with very heterogeneous droplet composition.

5 Effects of water condensation on polymer solution surface tension, dielectric permittivity and conductivity

As water condenses into the Taylor cone, many solution properties will change. While we argue in the main paper that the key change is in the quality of the solvent, here we look into the effects on surface tension γ, dielectric permittivity ϵ and conductivity σ as well.

5.1 Variations in surface tension

Starting with the surface tension of polymer-free water-ethanol solutions, Vasquez et al. published a rich set of data,[4] the relevant values at 20°C plotted in Figure S5. While γ increases with added water content, the increase is actually not very rapid. Only as we approach nearly pure aqueous solution, γ rises strongly. The surface tension stays below 25 mN/m until almost half of the liquid is water, and 30 mN/m is not reached until about 75 mol% water. The effects of water condensation into the Taylor cone related to surface tension can thus be expected to be rather low, being nearly negligible up to water concentrations where the reduction in solvent quality has a much greater impact. Moreover, as a change in γ would simply affect the spinning voltage slightly, it is of no relevance for the phenomena discussed in our study, namely Taylor cone gelation and multiple jet ejection.

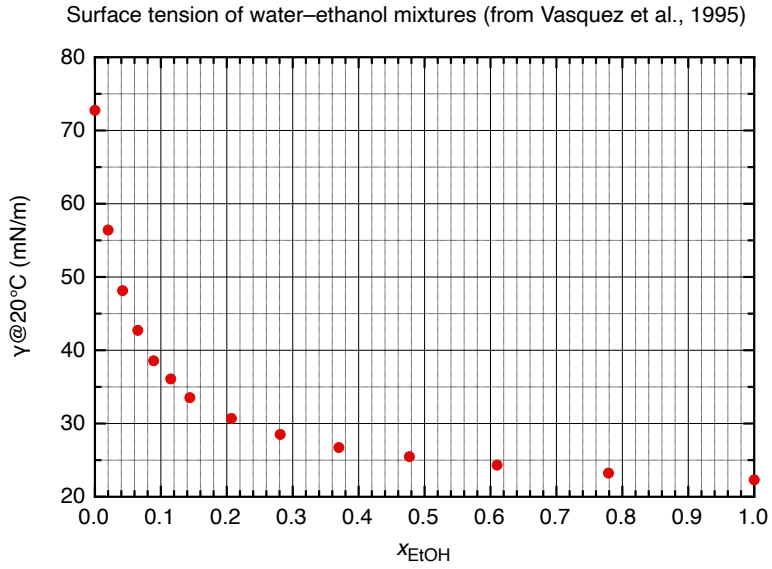

Figure S5: Surface tension γ at 20°C of water–ethanol mixtures as function of mole fraction of ethanol, the data obtained from Vasquez et al.[4]

5.2 Variations in conductivity

In order to check that no significant anomaly in conductivity occurs as water is condensing from the humid air into the ethanolic PVP solution we refer to the literature for data on conductivity of water-ethanol mixtures. For the mixtures of just the two solvents, without polymer, Personna et al. published a full data set that demonstrates a decrease of conductivity that follows a linear character in a plot of $\log(\sigma)$ versus volume fraction of ethanol in water,[5]

from slightly above 200 μS/cm for pure water to about 10 μS/cm at about 80% ethanol. The drop thereafter is more rapid down to about 1 μS/cm for pure ethanol. For mixtures with PVP added there are less data in the literature, but two papers also cited in the main article give some results also for mixed water-ethanol solvents. Asawahame et al. studied 12% PVP with $Mw = 1.3 \cdot 10^6$ g/mol, as in our study, reporting a conductivity increase from 11.9 to 22.0 to 26.6 "ms/cm" as the mixing ratio is changed from pure ethanol to 20% water to 30% water.[6] We assume that the unit of the data is a typo, and it should be μS/cm.

For PVP with $M_w = 0.36 \cdot 10^6$ g/mol, Cengiz Callioglu and Kesici Güler reported the conductivities for a 12% solution in pure ethanol, in 50/50 ethanol/water mixture, and in pure water, to be $\sigma = 8.6$, 23 and 87 μS/cm, respectively, thus higher conductivities for pure ethanol but lower for pure water compared to when no PVP is added, comparing with the Personna data mentioned above. The important conclusion is that in all cases the conductivity remains orders of magnitude greater than the LC core, hence little should change to the coaxial situation, and for the non-coaxial situation, the changes in σ might call for a slight adjustment of voltage, but they cannot give rise to the gelation in the Taylor cone and multiple jet ejection.

5.3 Variations in dielectric permittivity

The dielectric permittivity (dielectric constant) ϵ of water–ethanol mixtures was studied by Jeffries Wyman already in 1931.[7] The permittivity at 20°C decreases somewhat sublinearly from $\epsilon \approx 80$ for pure water to $\epsilon \approx 25$ for pure ethanol. The strongest deviation from linearity is around 60% ethanol, where $\epsilon \approx 43$ while a linear extrapolation between the values of pure water and ethanol, respectively, would yield $\epsilon \approx 47$. In other words, the behavior is quite close to linear and there are thus no spectacular anomalies in ϵ as water is added to ethanol. We expect the same conclusion to hold for water addition to the ethanolic PVP solution. Of course, the increasing ϵ as water is added affects the electrostatics, but the effect can easily be compensated for by adjusting the voltage. It cannot explain the phase separation phenomena that we observe and discuss here.

6 Diagrams of the electrospinning & coaxial spinneret setups

The diagrams of the electrospinning and coaxial spinneret setups discussed in the Experimental section of the main paper are shown in Figure S6 and Figure S7, respectively.

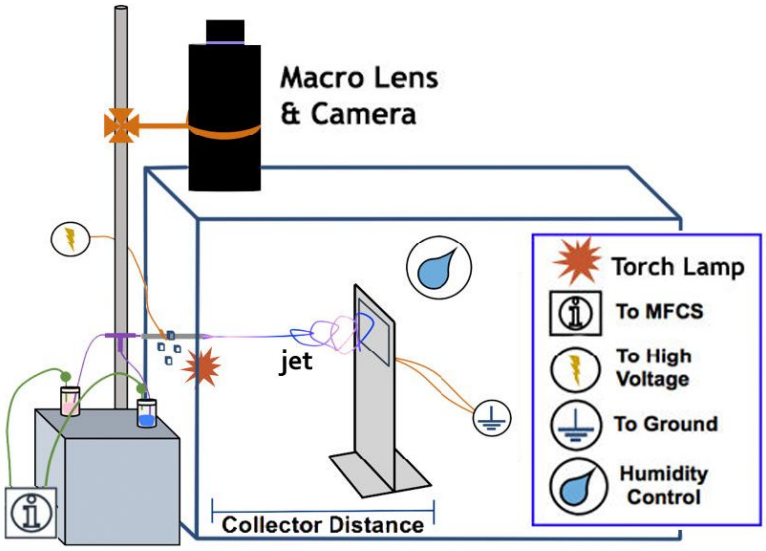

Figure S6: The line drawing of the coaxial electrospinning setup used to produce the fiber mats. Box dimensions are: 50 cm tall, 45 cm wide, and 45 cm long. The placement of the various components (see legend) are shown. The spinning takes place horizontally here. The MFCS is the microfluidic control unit governing the flow rate of the sheath and core liquids.

The line diagram and photograph of the coaxial spinneret setup in Figure S7 show how the individual components - tubes for flowing the PVP and LC, T-coupler, and stainless steel blunt-end capillary were fitted together, and how the final setup appears during use. The tube connections from the microfluidics pressure based flow control system (Fluigent MFCS-EZ) are also shown emerging from the tops of the vials. These tubes provided the air flow needed to transport the liquids into the coaxial spinneret.

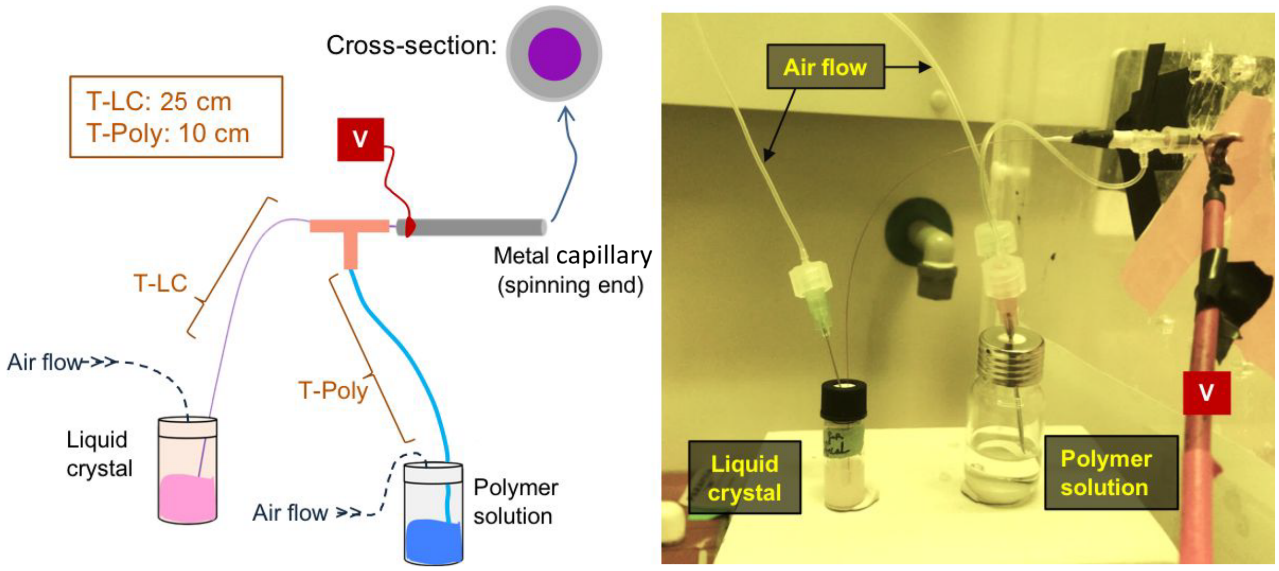

Figure S7: The coaxial spinneret setup used to electrospin the LC-PVP fibers, with a photograph (right) showing the setup during an actual experiment. Air from the flow control unit (MFCS-EZ) is passed into the vials containing the polymer solution and LC. Over-pressurizing the vials causes the fluids to flow through their respective tubes into the coaxial spinneret. The total length of the tube that flows the LC ("T-LC") out of the coaxial setup was 25 cm. Note that this tube is inserted into one end of the T-coupler (shown in orange) and passes through the metal capillary. The total length of the tube that flowed the polymer solution ("T-Poly") was 10 cm. This tube only goes from the solution vial up to the T-coupler and does not pass through the metal capillary. The potential ("V" for voltage) is connected to one side of the metal capillary so that the co-flowing solutions can be charged before exiting the tip. The end of the metal capillary cannot be seen in the photo because the wall of the spinning setup is covering that side.

7 How the half angles of the Taylor cones were measured

Figure S8 shows a representative coaxial Taylor cone analyzed using the *FIJI* program (downloadable here: https://imagej.net/Fiji)[i] to find its estimated cone half-angle. Here, the measured half-angle from the center of the cone to its base ($\measuredangle bef$ in Figure S8) is approximately 43° (shown in the window called "Results" on the right side of the image). To make this measurement, the image of the cone was opened in *FIJI* and several geometric shapes consisting of four points (a, b, c, e), a circle (d), and an angle were drawn on it as overlay features. Because the shapes were saved as overlays, they could be analyzed with respect to one another in the "region of interest" or ROI manager window (lower right side in Figure S8). The x and y pixel coordinates of the center of the yellow circle (d) drawn at the apex of the Taylor cone tip and its diameter were used to find the center point (e). At the base of the cone, points (a) and (c) were made to mark the top and bottom boundaries, and using their x and y coordinates, the center point (b) was found. Finally, using the angle tool (with symbol: $\sphericalangle$) from the "(FIJI is Just) ImageJ" main menu window, an angle was drawn from the points (b) to (e) to (f). The line drawn from (e) to (f) was chosen because it traces the straight-most side of the Taylor cone best.

[i] *FIJI* is a distribution of the original open source, Java-based image processing program *ImageJ* developed at the National Institutes of Health: https://imagej.nih.gov/ij/

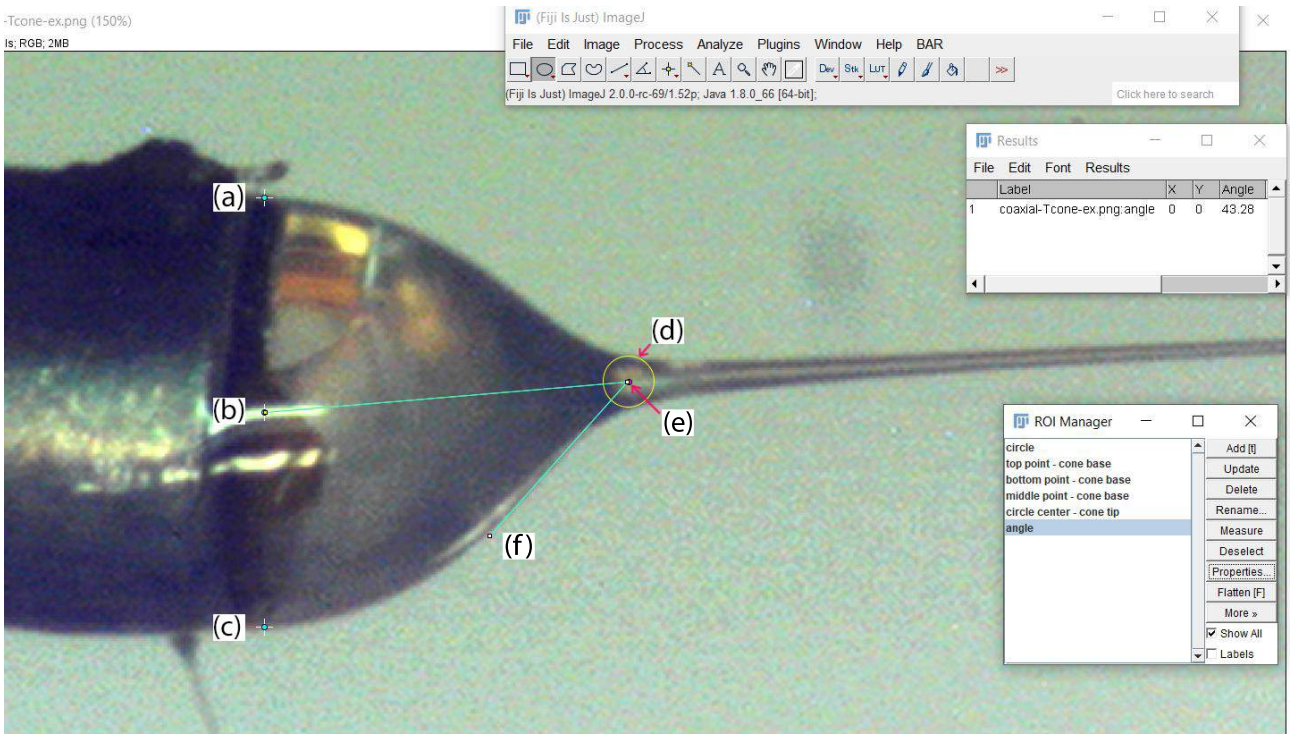

Figure S8: A representative Taylor cone image processed using the *FIJI-ImageJ* program to find the cone half-angle made at $\measuredangle bef$ is shown. Points (a), (b), and (c) mark the top-most, center, and bottom-most points of the base of the Taylor cone, while the center point of circle (d) is labeled as point (e). Point (f) marks on the straight-most side of the cone the end point of $\measuredangle bef$. The windows to the right of the image show the shapes and points can be individually analyzed, with the angle showing a measurement of 43.28° (≈43°).

Table S1 and Table S2 show additional Taylor cone half-angles measured for the PVP-ethanol solutions spun with and without the LCs at high and low (25%) RH. As the Taylor cones for the solutions containing the 5CB core were neither symmetrical, nor stable at 65% RH they were not analyzed using the method shown in Figure S8. However, measurements of the coaxial PVP-5CB cones at low RH were possible and had an average value of roughly 37° ± 5 °. To summarize, all half angles measured in both high and low RH range from about 35° to 43°, with the lower values and lower standard deviations, being present for the non-coaxial PVP cones. The applied voltages used to generate the cones measured here were 9.5kV for the coaxial types, and 9.0kV for the non-coaxial types.

Table S1: Additional measurements of the Taylor cone half angles formed from the PVP-ethanol solution (without a core fluid), the PVP-ethanol sheath solution with the E7 core, and the PVP-ethanol sheath with the ROTN-403 core at 65% relative humidity. The mean values and standard deviations are also shown.

Trial	PVP-ethanol (no core)	PVP+E7	PVP+ROTN-403
1	37.6°	36.0°	33.7°
2	35.1°	43.1°	42.3°
3	34.0°	36.0°	40.0°
Mean	35.6°	38.4°	38.7°
Std.Dev.	1.8°	4.1°	4.5°

Table S2: Additional measurements of the Taylor cone half angles formed from the PVP-ethanol solution with the 5CB core at 25% relative humidity. The mean value and standard deviation is also shown.

Trial	PVP+5CB
1	42.6°
2	35.1°
3	34.0°
Mean	37.2°
Std.Dev.	4.7 °

According to several studies, ideal Taylor cone half-angles range from 32° to 47°,[8–13] where the generally accepted criteria for defining an "ideal" and stable Taylor cone that produces continuous fibers is as follows:

- the Rayleigh-Plateau instability has been suppressed in the charged hanging drop so that it does not drip and has cone shape,
- the cone has not gelled or dried,
- the cone is symmetric,
- the cone does not pulse or disappear/reappear suddenly.

Examples of Taylor cones that have a distorted, asymmetrical shape and which have begun to dry out are shown in Figure S9(a) and (b). These are also examples for which using the method above to measure their half angles will not work.

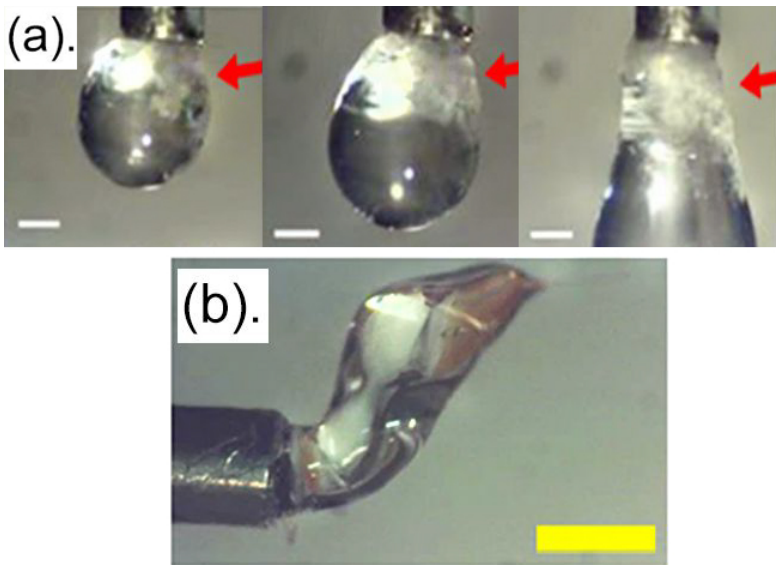

Figure S9: Representative coaxial Taylor cone images showing phase separation where the polymer is drying out of the solution used to spin as it exits the spinneret (a), and severe shape distortion (b). In (b) the cone part takes on an "s" cobra-like shape as the flowing outer sheath gelled and the inner core was still allowed to flow. The outcome was that the core fluid pushed the gelling sheath tube further outwards. The set of images labeled (a) were reprinted from Urbanski et al.[14] under the CC BY 3.0. Creative Commons license. Yellow scale bar: 1.1 mm; white scale bars: 0.5 mm.

References

[1] Reichardt, C. Empirical Parameters of Solvent Polarity from Spectroscopic Measurements. In *Solvents and Solvent Effects in Organic Chemistry, 3rd ed.*; Wiley-VCH: Weinheim, Germany, 2003; pp 441–443.

[2] Reichardt, C. Solvatochromic Dyes as Solvent Polarity Indicators. *Chem. Rev.* **1994**, *94*, 2319–2358.

[3] Reyes, C.; Baller, J.; Araki, T.; Lagerwall, J. Isotropic-Isotropic Phase Separation and Spinodal Decomposition in Liquid Crystal-Solvent Mixtures. *Soft Matter* **2019**, *15*, 6044–6054.

[4] Vazquez, G.; Alvarez, E.; Navaza, J. M. Surface Tension of Alcohol Water + Water from 20 to 50°C. *J. Chem. Eng. Data* **1995**, *40*, 611–614.

[5] Personna, Y.; Slater, L.; Ntarlagiannis, D.; Werkema, D.; Szabo, Z. Electrical Signatures of Ethanol-Liquid Mixtures: Implications for Monitoring Biofuels Migration in the Subsurface. *J Contam Hydrol* **2013**, *144*, 99–107.

[6] Asawahame, C.; Sutjarittangtham, K.; Eitssayeam, S.; Tragoolpua, Y.; Sirithunyalug, B.; Sirithunyalug, J. Formation of Orally Fast Dissolving Fibers Containing Propolis by Electrospinning Technique. *Chiang Mai Journal of Science* **2015**, *42*, 469–480.

[7] Wyman, J. The Dielectric Constant of Mixtures of Ethyl Alcohol and Water from -5 to 40°C. *J. Am. Chem. Soc.* **1931**, *53*, 3292–3301.

[8] de la Mora, J. F. The Effect of Charge Emission from Electrified Liquid Cones. *J. Fluid Mech.* **1992**, *243*, 561–574.

[9] Rulison, A. J.; Flagan, R. C. Scaleup of Electrospray Atomization using Linear Arrays of Taylor Cones. *Rev. Sci. Instrum.* **1993**, *64*, 683–686.

[10] Yarin, A. L.; Koombhongse, S.; Reneker, D. H. Taylor Cone and Jetting from Liquid Droplets in Electrospinning of Nanofibers. *J. Appl. Phys.* **2001**, *90*, 4836–4846.

[11] Reneker, D. H.; Yarin, A. L. Electrospinning Jets and Polymer Nanofibers. *Polymer* **2008**, *49*, 2387–2425.

[12] Andrady, A. Description of Electrostatic Spinning. In *Science and Technology of Polymer Nanofibers*; John Wiley & Sons, Inc.: Hoboken, NJ, USA, 2008; pp 9–22.

[13] Barua, B.; Saha, M. C. Investigation on Jet Stability, Fiber Diameter, and Tensile Properties of Electrospun Polyacrylonitrile Nanofibrous Yarns. *J. Appl. Polym. Sci.* **2015**, *132*, 41918–41929.

[14] Urbanski, M.; Reyes, C. G.; Noh, J.; Sharma, A.; Geng, Y.; Subba Rao Jampani, V.; Lagerwall, J. P. F. Liquid Crystals in Micron-Scale Droplets, Shells and Fibers. *J. Phys. Condens. Matter* **2017**, *29*, 133003.